Geometry effect on membrane absorption for CO_2 capture.

Part I: A hybrid modeling approach

*Kaiyun Fu, Sunyang Wang, Zhenbin Gu, Yushu Liu, Tianming Zai, Shijie Li, Xianfu Chen, Minghui Qiu, Yiqun Fan**

State Key Laboratory of Materials-Oriented Chemical Engineering, College of Chemical Engineering, Nanjing Tech University, No.30 South Puzhu Road, Nanjing 211816, P.R. China

*Corresponding author:

E-mail address: yiqunfan@njtech.edu.cn (Y. Fan)

Abstract

Membrane absorption (MA) has a great prospect for CO_2 capture. In MA modeling, conventional 1D- and 2D- models make simplification of membrane contactor (MC) geometry. Geometry simplification allows an easy process modeling and numerical solution, however, is only reasonable for particular MCs. Here, efforts are underway to quantify the geometry effect on the MA-CO_2 performance. First, we proposed a full 3D model without geometry simplification for simulating the MA-CO_2 process in real MCs and then validated it with experimental data. More importantly, we highlighted a preferable hybrid model in which a correction factor (F) was introduced to the 2D simulation results to make their combination approximately equal to the 3D simulation values. The F was correlated with dimensionless parameters obtained from computational fluid dynamics (CFD) studies for characterizing the geometry effect. Such hybrid modeling contributes to characterizing the influence of geometry on the MA-CO_2 performance and improving computation accuracy-efficiency combinations.

Keywords: Membrane contactor; Absorption; Modeling; Mass transfer; Geometry effect

1 Introduction

Efforts to reduce carbon dioxide (CO_2) emission rely on the development of advanced CO_2 capture technologies. Membrane contactor (MC) has received considerable attention in past two decades for CO_2 or sulfur dioxide (SO_2) absorption owing to its high interfacial area for mass transfer, flexible installation and operation, and easy device-modularity, etc.[1-3]

In the past decades, extensive lab-scale studies have been reported on membrane absorption (MA) for CO_2 capture using various membrane materials such as polypropylene (PP)[4] and polytetrafluoroethylene (PTFE)[5-8], and chemical solvents such as monoethanolamine (MEA),[4] and 4-diethylamino-2-butanol (DEAB).[9] In addition, some effective approaches are used to reduce the mass transfer resistance of membrane element, such as preparing membranes with notable hydrophobicity (to prevent membrane wetting)[10] and with asymmetric structure (to increase permeability).[11] Moreover, substantial research efforts have contributed towards experimental measurement and numerical simulation to investigate the effects of membrane properties and operating conditions on the MA-CO_2 performances.[12] As the accumulation of fundamental data and the advance of MA technology, the number of tubes incorporated into the module increases from one or several tubes, as used in most lab-scale studies, to dozens and hundreds, or even more.[13] It is an important and indispensable step for MA-CO_2 technology tending towards industrial application.

A key challenge in the scaling up of MCs is an increasingly complex geometry which has a great effect on the gas and liquid flow behaviors. Some nonideal flow phenomena that might be insignificant in a lab-scale MC can not be neglected in a pilot or full-scale one, such as stagnant

regions (dead zones), bypass and short-circuiting. They are especially serious in the positions around inlet and outlet (so-called edge effects). Moreover, membrane elements are generally limited in length due to the characteristics of membrane materials (not good enough in either strength or toughness, or even both). Consequently, a pilot- or large-scale MC usually has a small height-to-diameter ratio, existing serious geometry effect. The geometry effect will affect the spatial distributions of velocity, concentration and temperature, and therefore affect the reaction of CO_2 and absorbent. Hence, not only the properties of absorbent and membrane material, but also the effect of MC geometry needs to be deeply investigated. As far as we know, few studies with respect to how MC geometry affects membrane CO_2 absorption performance can be found in literature.

Modeling and simulation can contribute to representing the MA process, optimizing operational condition and device geometry, and are important to direct MC scale-up. Up to now, most studies on modeling MA-CO_2 process involve either 1D or 2D models.[14-16] The 1D models are based on mass transfer resistance-in-series approach, while the 2D models are based on Navier–Stokes equations.[1] By comparison, 2D models can represent parameter variations in axial and radial directions, and therefore, become increasingly popular. Nevertheless, conventional 1D and 2D models are proposed based on simplified MC geometry, as illustrated in **Figure 1**, and then incapable of modeling nonideal flows induced by complex 3D geometry. These simplifications might be acceptable in case of using a MC with a large height-to-diameter (H/D) ratio and a small amount of membrane tubes, as used in most lab-scale studies. However, oversimplifications of MC geometry will give rise to large and nonlinear prediction errors in scaling up MC. Moreover, they are adverse to evaluate the performance of absorbent and membrane and to provide improved approaches for process intensification. For example, suppose there is a certain deviation between experiment data

and simulation results obtained from a 2D model, to what can be ascribed the deviation, a geometry effect, a membrane wetting or an inaccurate correlation of absorbent physicochemical properties? Therefore, more advanced approaches must be applied to address the complex problem of geometry effect on fluid flows.

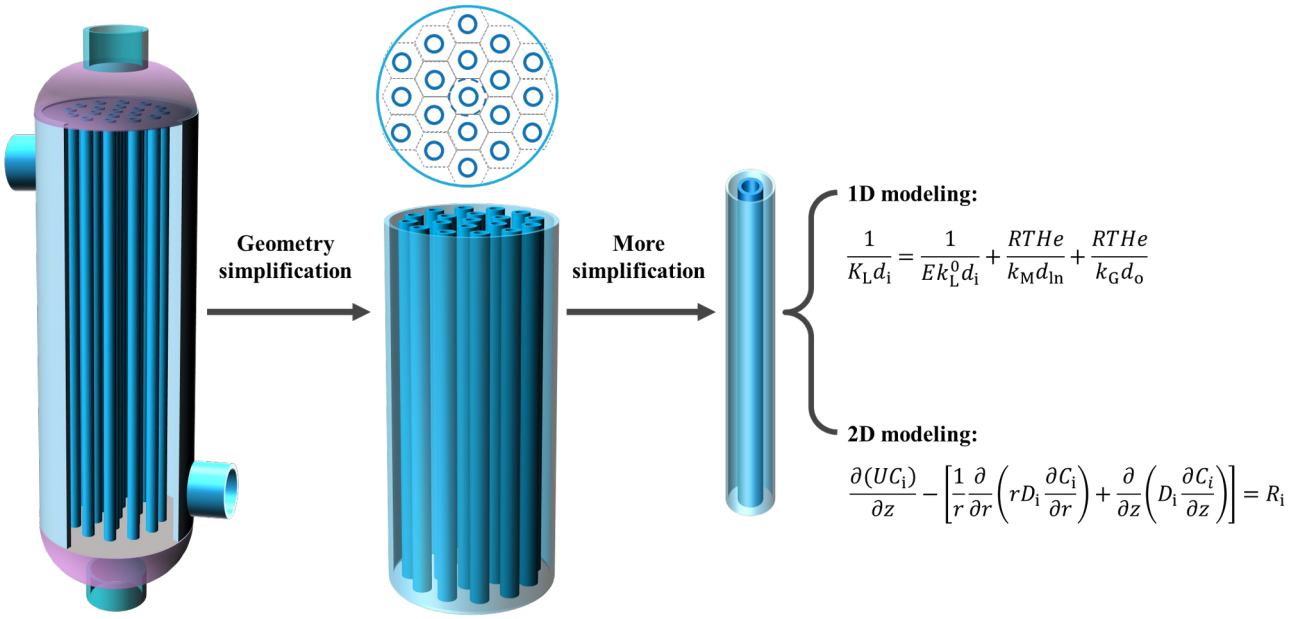

Figure 1. Conventional 1D and 2D approaches for modeling membrane absorption process

Almost all modeling and simulation exhibit a trade-off between accuracy —i.e., to what extent a model provides desired results—and efficiency—i.e., what processor and how long are required to complete a simulation task. A 3D modeling would probably enable it to represent a mass transfer process in a MC with complex geometry. Nevertheless, it concurrently requires a higher performance processor and longer calculation time compared to a 2D modeling. Essentially, CO_2 absorption into a chemical absorbent in a MC is a complex process. It involves a multiscale attribute, from molecular scale (chemical kinetics, chemical equilibrium and phase equilibrium) to mesoscale (the microstructure and interface of membrane material, and the mass transfer in pores) and to macroscale (the reacting fluids flowing in a MC with a specific geometry). Considering

simultaneously complex geometry and complex process, rigorous 3D-based computational simulations of reactive MA-CO_2 processes in multi-tube MC are still big problems with current computing power, or at least very impractical. How to maximize the trade-off is therefore critical for the design and optimization of MCs.

In this series of articles, we treat the MA-CO_2 process as a 3D problem and attempt to quantify the impact of MC geometry on the MA-CO_2 performance. In this part, we first presented a 2D and a 3D modeling approaches for the simulation of the membrane CO_2 absorption in aqueous MEA solution and validated them with experimental data. The prediction errors of the two approaches under various situations were compared and discussed. In addition, to improve simulation efficiency while also maintaining accuracy, we modified the 2D model by introducing an adjustable correction factor (F) to characterize the geometry effect. Finally, the F was determined and then correlated with dimensionless parameters.

2 A hybrid modeling approach

In the modeling of MA process based on Navier-Stokes equations, convection and diffusion are taken into account in the gas and liquid phases; chemical reaction is considered in the liquid phase; only mass diffusion takes place inside the membrane. Accordingly, gas and liquid flow fields, which could be significantly affected by MC geometry, play key roles in the MA process. Separation of the influence caused by geometry from other effects induced by absorbent and membrane material is expected to be an effective strategy for better understanding the multi-factor coupling process and proposing intensification approaches.

In this work, we first presented a 2D and a 3D models, respectively, to simulate the reactive MA-CO_2 process under various situations. Their simulation results were compared to the

experimental data presented in terms of CO_2 removal efficiency (η) which can be calculated with Eq. 1. Accordingly, the 2D and 3D simulation results and the experimental data were denoted as η_{2D}, η_{3D} and η_{exp}, respectively.

$$\eta = \left(1 - Y_{A,out}/Y_{A,in}\right) \times 100\% \quad (1)$$

where $Y_{A,in}$ and $Y_{A,out}$ are inlet and outlet mole ratio of CO_2, respectively.

Theoretically, a 3D mass transfer model for reactive MA-CO_2 process is available, however, is difficult, at least unpractical, to solve because of simultaneous challenges of complex process and complex geometry. Changing approach from a complex 3D MA modeling to that consists of two or several easily achievable steps can make related numerical models more solvable. Given that, we proposed an alternative approach in which a non-constant correction factor (F), obtained from computational fluid dynamics (CFD) studies for characterizing irregular flow behaviors under the influence of MC geometry, was introduced to the η_{2D} for the η_{3D} prediction. So the determination of F involves a simple process and a complex geometry. Note that many variables will affect F, major or minor, including the properties of the gas and liquid fluids (i.e., flow rates, temperatures, densities and viscosities) and the MC geometry (i.e., the sizes of tube and module, the number of membrane tubes, a tube pitch etc). Putting too many variables into a correlation for predicting F ends up reducing accuracy. Then, problem appears: how to associate the F with fewer variables while ensuring that it has reasonable physical meaning.

Considering that the gas phase flowing in the shell side is continuous and nonideal, its flow behavior can be characterized with residence time distribution (RTD). The RTD is a key concept in the subject of chemical reaction engineering and often employed to diagnose the flow characteristics of a reactor. In RTD researches and applications, a key parameter, i.e., dimensionless variance (σ_θ^2), is

often used to quantify flow characteristic and develop predictive model. In this work, experimental and simulation studies on gas-phase RTD were performed to determine the σ_θ^2 under various situations.

The features of liquid fluid in the tube side are different from those in the shell side. In the tube side entrance region, the concentrations and temperature are the same as the feed conditions, so the concentration and temperature fields are uniform; while the velocity field will be affected by geometry, resulting in uneven flow distribution for each membrane tube. In tube regions, each tube has a high length-to-diameter ratio, which allows fluid to present regular flow characteristics (the same as those supposed in the 2D modeling). Moreover, the fluid in each tube is independent and will not exchange material with those in other tubes. Therefore, the geometry effect on tube-side fluid mainly exhibits in uneven distribution of absorbent. In this work, the relative standard deviation (RSD) of the liquid flow rate for each tube was used to characterized the geometry effect on tube-side fluid.

Based on the description above, the flow diagram for quantifying the geometry effect on MA performance can be presented in **Figure 2**.

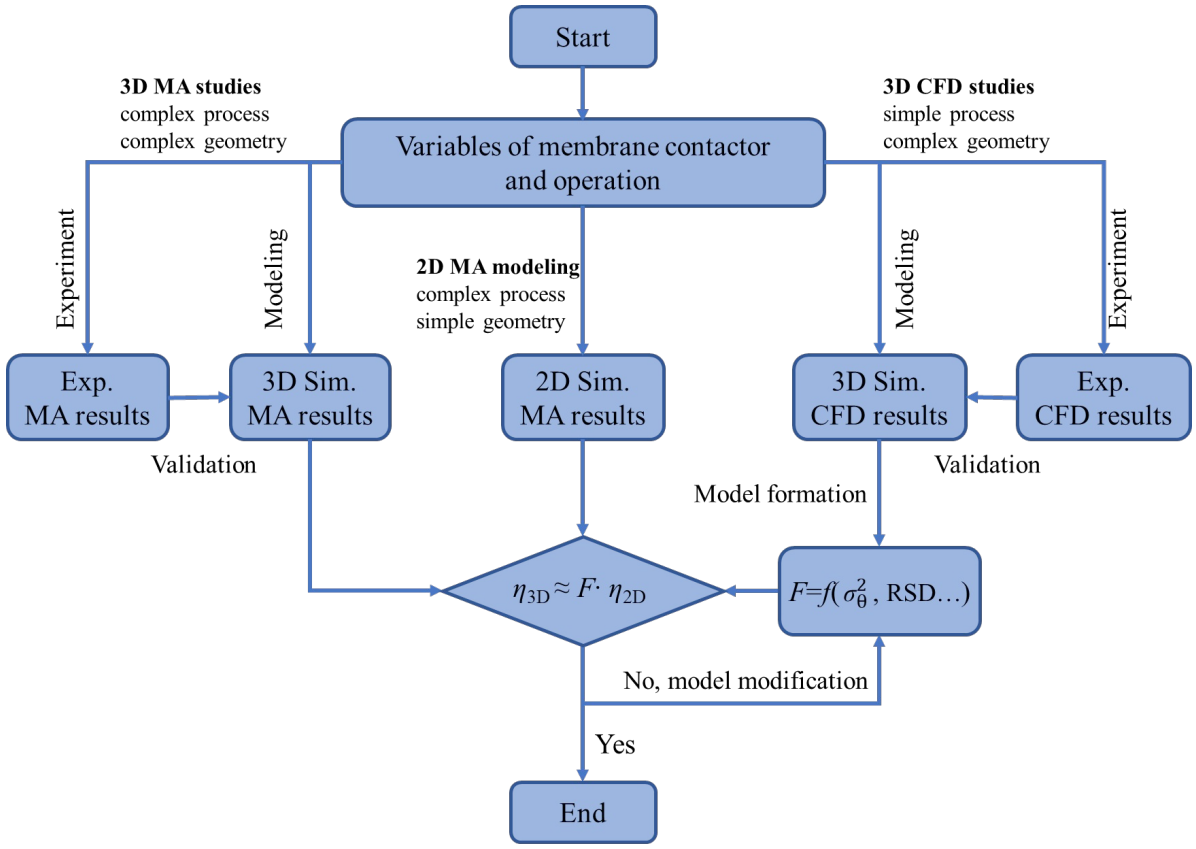

Figure 2. The development of a hybrid modeling approach for 3D reactive membrane absorption process

3. Modeling and simulation

Generalized Navier-Stokes equations were used for modeling the mass transfer within the MCs. Both 2D and 3D modeling approaches were employed to simulate the membrane absorption process and a 3D-based modeling approach was performed for the CFD studies. The modeling processes are presented below.

3.1 A 2D modeling of membrane absorption process

In this work, a typical 2D modeling approach for a simplified MC was developed based on following assumptions, as illustrated in **Figure 3**.

(1) The geometric structure of the inlets and outlets of the MC was ignored.

(2) The membrane tubes were uniformly arranged in hexagonal-shaped unit cells and each hexagon was approximately considered as a circle.

(3) The gas and liquid flow rates for each tube were equal.

(4) The reacting fluids flowing with fully developed laminar parabolic velocity profiles.

(5) The angular gradients of operating properties were negligible, so a 2D axisymmetric model was used.

(6) The gas phase was considered ideal, and the liquid was considered to be a Newtonian fluid.

(7) The CO_2 concentration at gas-liquid interface was consistent with Henry's law.

(8) Non-wetted condition.

(9) The membrane absorption process was operated at steady state.

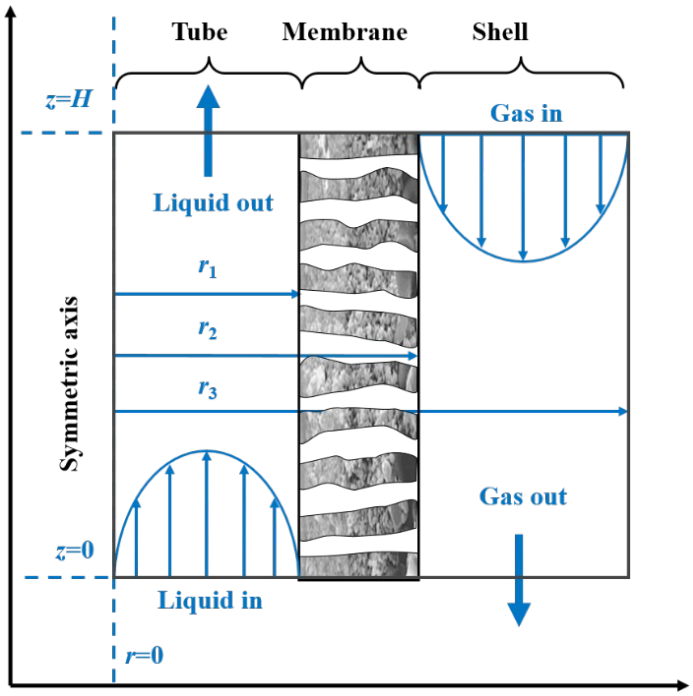

Figure 3. Schematic representation of membrane absorption via 2D model

The membrane CO_2 absorption process occurs in three distinct domains: tube side, membrane layer and shell side, as schematized in **Figure 3**. The 2D models were shown as follows.

—Tube side:

$$\frac{\partial(U_L C_{CO_2,L})}{\partial z} - \left[\frac{1}{r}\frac{\partial}{\partial r}\left(rD_{CO_2,L}\frac{\partial C_{CO_2,L}}{\partial r}\right) + \frac{\partial}{\partial z}\left(D_{CO_2,L}\frac{\partial C_{CO_2,L}}{\partial z}\right)\right] = R_{CO_2} \quad (2a)$$

where U_L is liquid velocity, m/s; $D_{CO2,L}$ and $C_{CO2,L}$ are the diffusion coefficient and concentration of CO_2 in the liquid phase, m^2/s and mol/m^3, respectively; R_{CO2} is the reaction rate of CO_2, $mol/(m^3 \cdot s)$; and r and z are the radius distance to the central axis and the axial coordinates, respectively, m.

—Membrane layer:

$$D_{CO_2,m}\left[\frac{\partial^2 C_{CO_2,m}}{\partial r^2} + \frac{1}{r}\frac{\partial C_{CO_2,m}}{\partial r} + \frac{\partial^2 C_{CO_2,m}}{\partial z^2}\right] = 0 \quad (2b)$$

Where $D_{CO2,m}$ and $C_{CO2,m}$ are the diffusion coefficient and concentration of CO_2 in the membrane layer, m^2/s and mol/m^3, respectively.

—Shell side:

$$\frac{1}{r}\frac{\partial}{\partial r}\left(rD_{CO_2,s}\frac{\partial C_{CO_2,s}}{\partial r}\right) + \frac{\partial}{\partial z}\left(D_{CO_2,s}\frac{\partial C_{CO_2,s}}{\partial z}\right) = 0 \quad (2c)$$

where $D_{CO2,s}$ and $C_{CO2,s}$ are the diffusion coefficient and concentration of CO_2 in the shell side, m^2/s and mol/m^3, respectively.

—Gas thermal balance:

$$\rho_G C p_G v_G \frac{\partial T_G}{\partial z} - \lambda_G\left(\frac{1}{r}\frac{\partial}{\partial r}\left(r\frac{\partial T_G}{\partial r}\right) + \frac{\partial^2 T_G}{\partial z^2}\right) = 0 \quad (3a)$$

—Membrane thermal balance:

$$\lambda_{M,eff}\left(\frac{1}{r}\frac{\partial}{\partial r}\left(r\frac{\partial T_M}{\partial r}\right) + \frac{\partial^2 T_M}{\partial z^2}\right) = 0 \quad (3b)$$

, where $\lambda_{M,eff} = \lambda_M(1-\varepsilon) + \lambda_G\varepsilon$

—Liquid thermal balance:

$$\rho_L Cp_L U_L \frac{\partial T_L}{\partial z} = \lambda_L \left[\frac{1}{r} \frac{\partial}{\partial r} \left(r \frac{\partial T_L}{\partial r} \right) + \frac{\partial^2 T_L}{\partial z^2} \right] + R_{CO_2} \Delta H_r \quad (3c)$$

where ρ_G and ρ_L are gas and liquid densities, respectively, kg/m^3; Cp_G and Cp_L are the specific heat of gas and liquid phases, J/(mol·K); T_G and T_L are the temperatures of gas and liquid phases, K; λ_G, $\lambda_{M,eff}$, λ_M, and λ_L are thermal conductivities of gas, membrane, and liquid phase, W/(m·K).

The boundary conditions for the above differential equations are presented in **Table 1**.

Table 1 The boundary conditions for the 2D differential equations

Boundary condition	Mass transfer	Heat transfer
At r=0	$\partial C_{i,L}/\partial r = 0$	$\partial T_{i,L}/\partial r = 0$
At r=r_1	$C_{CO_2,L} = C_{CO_2,m} RT / H_{CO_2,L}$	$T_L = T_M$
At r=r_2	$C_{i,M} = C_{i,G}$	$T_L = T_{L0}$
At r=r_3	$\partial C_{i,L}/\partial r = 0$	$\partial T_{i,L}/\partial r = 0$
At liquid inlet	$C_{i,L} = C_{i0,L}$	$T_L = T_{L0}$
At liquid outlet	$\partial C_{i,L}/\partial z = 0$	$\partial T_{i,L}/\partial z = 0$
At gas inlet	$C_{i,G} = C_{i0,G}$	$T_G = T_{G0}$
At gas outlet	$\partial C_{i,G}/\partial z = 0$	$\partial T_G/\partial z = 0$
At z=0 and H, r=r_1~r_2	$\partial C_{i,M}/\partial z = 0$	$\partial T_M/\partial z = 0$

where r_1~r_3 are the inner and outer diameters of the membrane and the inner diameter of the module, respectively, m; R is the gas constant, J/(mol·K); $H_{CO2,L}$ is the Henry's Law constant, Pa·m^3/mol.

3.2 A 3D modeling of membrane absorption process

For the 3D-based MA modeling, it was similar to that of the 2D modeling, except that the MC geometry was fully taken into account. In this work, a 3D modeling approach was developed in terms of rectangular coordinate based on the following assumptions:

$$\nabla \cdot C_{i,G} U_L - D_{AB} \nabla^2 \cdot C_{i,G} = 0 \quad (4a)$$

$$D_{i,M} \nabla^2 \cdot C_{i,M} = 0 \quad (4b)$$

$$\nabla \cdot C_{i,L} U_L - D_{i,L} \nabla^2 \cdot C_{i,L} = R_i \quad (4c)$$

Equations 5a-5c are the heat transfer models for gas, membrane and liquid phases, respectively.

$$\rho_G Cp_G \nabla \cdot (U_G T_G) - \lambda_G \nabla^2 \cdot T_G = 0 \quad (5a)$$

$$\lambda_{M,eff} \nabla^2 \cdot T_{i,M} = 0 \quad (5b)$$

$$\rho_L Cp_L \nabla \cdot (U_L T_L) = \lambda_{GL} \nabla^2 \cdot T_{GL} + R_{CO_2} \Delta H_r \quad (5c)$$

Boundary conditions for the 3D model are designated in terms of surfaces, rather than those for the 2D model in terms of lines. They are defined as follows:

At the membrane tube's outer surface: $C_{i,G}=C_{i,M}$, $T_G=T_M$;

At the membrane tube's outer surface: $C_{i,M}=C_{i,L}$, $T_M=T_L$;

At the inlets of the gas and liquid phases: $C_{i,G} = C_{i0,G}$, $T_G = T_{G0}$; $C_{i,L} = C_{i0,L}$, $T_L = T_{L0}$.

3.3 Flow characteristics obtained from CFD simulation

In this work, step tracer simulation was employed to obtain the σ_θ^2 of gas phase. The step method is to switch the fluid that flows constantly in the MC at time t=0 to the fluid containing a certain concentration of tracer (C_0) with the same flow rate. Then, the outlet tracer concentration $C(t)$ versus t is continuously recorded until the $C(t)$ is indistinguishable from the C_0.

Generally, a cumulative distribution function, F(t), is defined as a normalized response to the step input. Stated symbolically, the F(t) curve can be presented as follows.

$$F(t) = C(t)/C_0 \tag{6a}$$

The mean residence time (t_m) can be calculated as follows.

$$t_m = \int_0^\infty t \frac{dF(t)}{dt} dt \tag{6b}$$

The variance, or square of the standard deviation. It is defined by

$$\sigma_t^2 = \int_0^\infty (t - t_m)^2 \frac{dF(t)}{dt} dt \tag{6c}$$

Dimensionless variance can be defined by

$$\sigma_\theta^2 = \sigma_t^2 / t_m^2 \tag{6d}$$

For liquid flow, the RSD of the liquid flow rate for all tubes can be calculated as follows:

$$\text{RSD} = \frac{\sqrt{\frac{1}{n}\sum_{i=1}^{n}\left(u_{Li} - \overline{u_L}\right)^2}}{\overline{u_L}} \tag{7}$$

where n is the number of tubes; u_{Li} and $\overline{u_L}$ are the flow rate of tube i and the average liquid flow rate, respectively, m^3/s.

3.4 Physicochemical properties of fluids

3.4.1. Chemical reactions

Based on zwitterion mechanism, the chemical reactions of CO_2–MEA aqueous system are governed by the following equations: [17,18]

$$\text{MEA} + \text{H}^+ \xleftrightarrow{k_1, k_{-1}} \text{MEAH}^+ \tag{8a}$$

$$\text{CO}_2 + \text{MEA} \xleftrightarrow{k_2, k_{-2}} \text{MEA}^+\text{COO}^- \tag{8b}$$

$$\text{CO}_2 + \text{H}_2\text{O} \xleftrightarrow{k_3, k_{-3}} \text{HCO}_3^- + \text{H}^+ \tag{8c}$$

$$CO_2 + OH^- \xleftrightarrow{k_4, k_{-4}} HCO_3^- \quad (8d)$$

$$HCO_3^- \xleftrightarrow{k_5, k_{-5}} H^+ + CO_3^{2-} \quad (8e)$$

$$H_2O \xleftrightarrow{k_6, k_{-6}} OH^- + H^+ \quad (8f)$$

where k_i and k_{-i} are the forward and reverse rate constants of reaction (*i*), respectively. The Eqs. 8b and 8d are considered to be reversible with finite reaction rates, whereas the Eqs. 8a, 8c, 8e and 8f are considered to be reversible, instantaneous, and at equilibrium because they involve only proton transfer.[19]

3.4.2. Physicochemical properties

The physicochemical properties of fluids such as diffusivity, viscosity, density and Henry's law constant were estimated using correlations available in literature. These key properties are presented in **Table 2**.

Table 2 Physicochemical properties of the gas and liquid phases and membrane material.

Properties	**Units**	**Literature resources**		
		Gas	Liquid	Membrane
Specific heat	*Cp* [J/(mol·K)]	Welty et al.[20]	Weiland et al.[21]	—
Diffusion coefficients	D_i [m^2/s]	Welty et al.[20]	Versteeg et al.[22], Ko et al.[23]	Welty et al.[20]
Heat of absorption	ΔH_{abs} [J/mol]	—	Kim and Svendsen[24]	—
Density	ρ [kg/m^3]	Perry et al.[25]	Weiland et al.[26]	—
Viscosity	μ [Pa/s]	Perry et al.[25]	Weiland et al.[26]	—
Thermal conductivity	λ [W/(m·K)]	Reid et al.	Perry et al.[25]	Perry et al.[25]
Surface tension	γ [N/m]	—	Vazquez et al.[27]	—
Reaction rate constants	k_i	—	Hikita et al.[28]	—
Equilibrium constants	K_i	—	Edwards et al.[29]	—
Henry's constant	*He*	—	Glasscock et al.[30]	—

3.5 Numerical solution

The simulations of the proposed 2D- and 3D- MA models and 3D CFD simulation were performed using COMSOL Multiphysics which is powerful for solving engineering problems based on the finite element method (FEM). Four kinds of physical fields within the COMSOL software were coupled to simulate the reactive MA process, including: i. *Laminar Flow*, ii. *Transport of Diluted Species*, iii. *Chemistry*, iv. *Heat transfer in Solids and Fluids*. Two physical fields, i.e., *Laminar Flow* and *Transport of Diluted Species*, were coupled to investigate the CFD stuides. Grid independence tests have been performed to ensure that the simulation results are independent of the mesh size.

4. Experiment section

4.1 Materials

Commercial grade CO_2 and N_2 with purities of ≥ 99.9% were obtained from Jiangsu Tianhong Chemical Co., Ltd., China. Monoethanolamine (MEA) with purities of ≥ 99% was purchased from Xilong Chemical Co., Ltd., China. Deionized water was homemade (electrical conductivity <12 $\mu S \cdot cm^{-1}$). Tubular ceramic membranes were supplied by Jiuwu Hi-Tech Co., Ltd. These ceramic membranes have asymmetric structures composed of (i) a substrate with an average pore diameter of 1.0 μm and a thickness of 1.0 mm and (ii) a top layer with an average pore diameter of 100 nm and a thickness of 20 μm. The membrane element has a porosity of 0.4 and a tortuosity of 2.5. The ceramic membranes were modified to achieve hydrophobicity. The detailed procedures of hydrophobic

modification can be found in our previous work [31].

Three modules packed with different numbers of membrane tubes were used to validate the proposed models. The specifications of the membrane contactors are listed in **Table 3** and the images of them are shown in **Figure 4**.

Table 3 The geometrical sizes of the membrane contactors used in the work

Parameters	Unit	MC-1	MC-7	MC-19
Module ID.	(mm)	10	40	65
Number of tube		1	7	19
Shell side length	(cm)	23	23	23
Tube OD.	(mm)	6.0	6.0	6.0
Tube ID.	(mm)	4.0	4.0	4.0

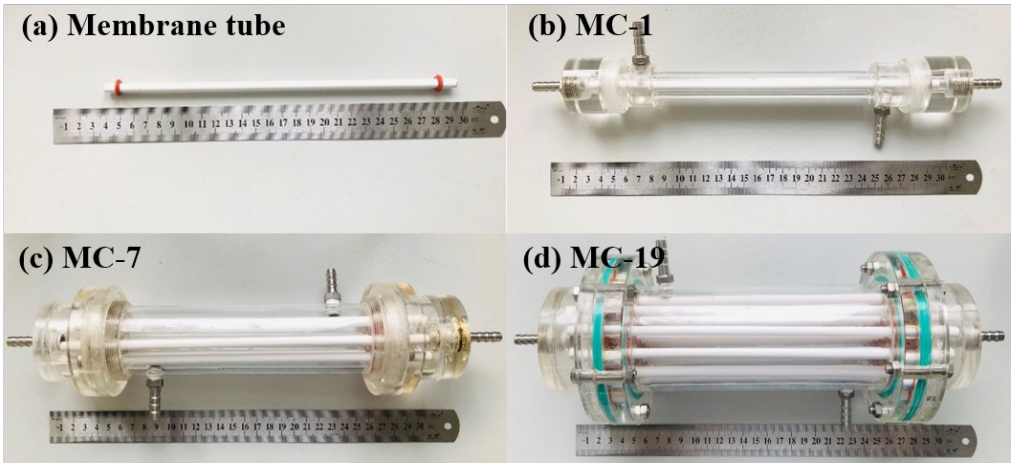

Figure 4. Images of (a) membrane tube, (b) MC-1, (c) MC-7 and (d) MC-19

4.2 Experimental setup and operation

(1) Membrane absorption experiment

A schematic of the experimental setup for membrane absorption is presented in **Figure 5**. The membrane absorption experiments were performed under countercurrent operation. A gas mixture (10 vol.% CO_2 and 90 vol.% N_2) was prepared by combining pure N_2 and CO_2 from cylinders. The gas flow rates were controlled by mass flow controllers (MFC, D07-19B, Beijing Sevenstar

Electronics Co., Ltd., China). The gas mixture was introduced into the shell side of the membrane contactor. Aqueous MEA solution was driven by a graduated cylinder and fed into the tube side of the membrane module at desired liquid flow rates. Both the gas and liquid fluids were preheated and controlled by water-bath heaters. The outlet temperatures of the gas and liquid phase, the outlet CO_2 concentration were measured at the steady state. Finally, liquid samples were taken and analyzed to determine the CO_2 loading. To confirm the validity of each experimental run, a mass balance calculation was conducted. The mass balance errors for all runs were found to be less than 3%.

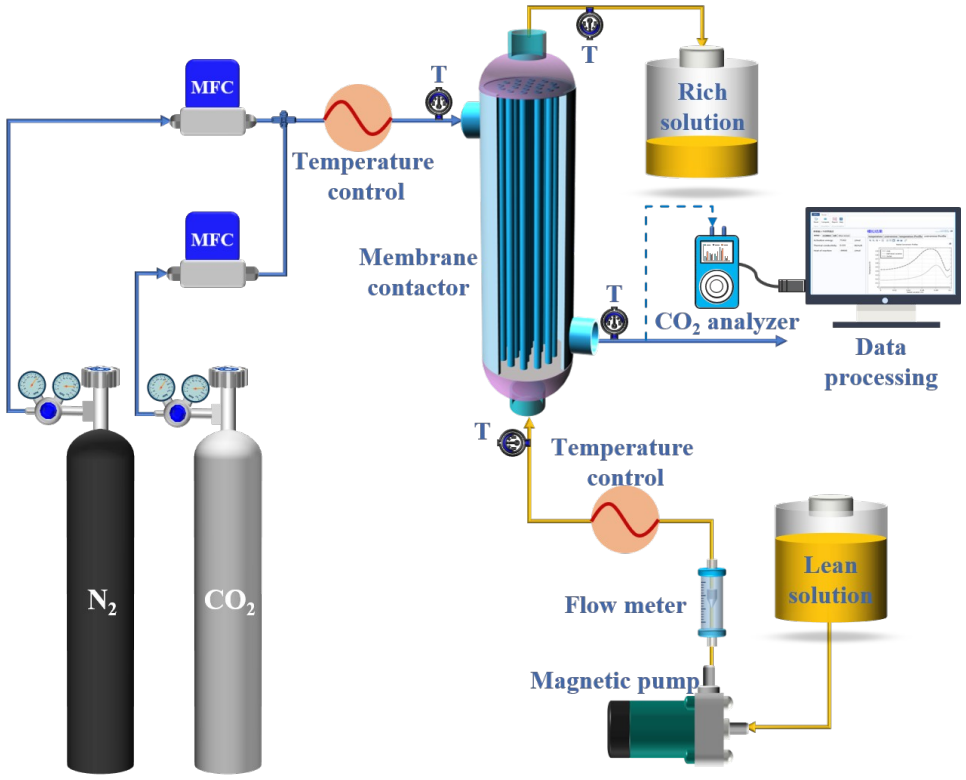

Figure 5. Schematic diagram of CO_2 absorption experiment apparatus

The experiment setups for the determination of gas and liquid fluid flow characteristics were illustrated in **Figure 6**. A step tracer method was used for the gas RTD determination, as shown in Figure 6a. A gas flow of pure N_2 was first preheated and controlled by a water-bath heater and steadily fed into the shell side of the membrane contactor and then, at time t=0, was replaced by a

gas mixuture of N_2 and CO_2 with the same temperature and flow rate. Then, the outlet CO_2 concentration versus t was continuously recorded until it reached the inlet value. Throughout the process, the tube side of the membrane contactor was filled with CO_2-saturated water to prevent CO_2 lose. Figure 6b shows the schematic of liquid flow characteric determination. To obtain the liquid RSD, the liquid flow rates of all tubes were determined respectively for the the liquid RSD calculated with Eq. 7. The liquid flow rate was determined by measuring a known volume of liquid versus time.

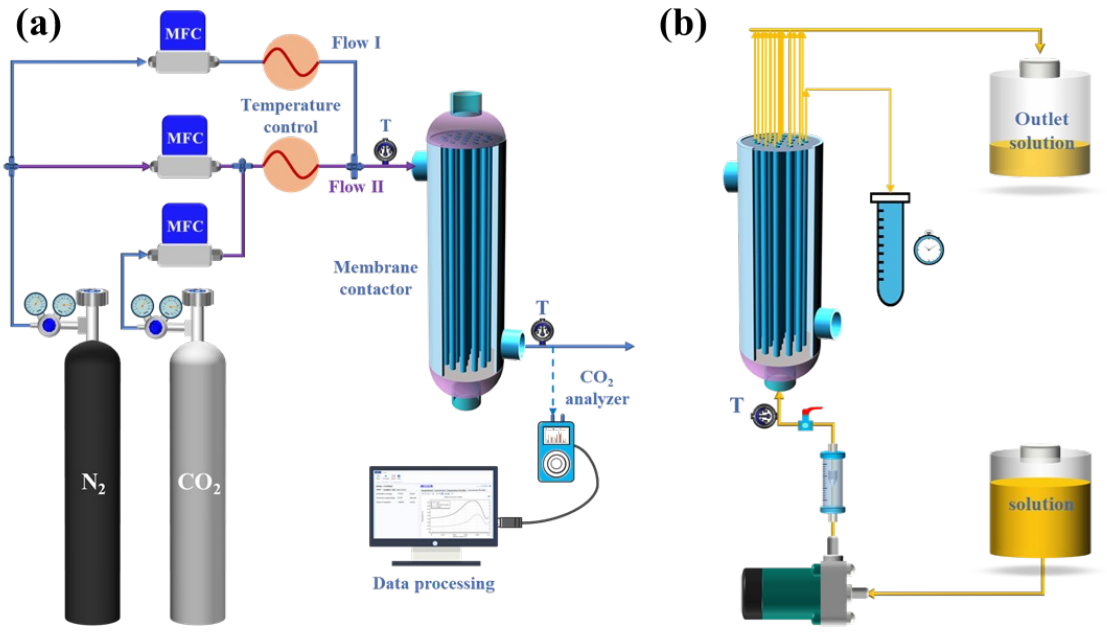

Figure 6. Schematic diagram of the experiment apparatus for (a) gas RTD and (b) liquid RSD determinations

The operating conditions for MA and fluid flow experiments are presented in **Table 4**.

Table 4 Experimental operating conditions.

Parameters	Unit	Membrane absorption	Fluid flow
MCs		MC-1, MC-7, MC-19	MC-7, MC-19
Gas flow rate	(ml/min)	100~950	100~950
Inlet CO_2 concentration	(%)	10.0	5.0
Inlet gas temperature	(℃)	20~40	20~40

Liquid flow rate	(ml/min)	10~200	10~200
Inlet liquid temperature	(ºC)	20~40	20~40
MEA concentration	(mol/L)	1.0~5.0	—
CO_2 loading	(mol/mol)	0~0.2	—

4.3 Sample Analysis.

The concentration of MEA solution was verified by titration with a known volume of 1.0 mol/L hydrochloric (HCl), with methyl orange as an indicator. The CO_2 loading in liquid sample was determined by the standard method given by the Association of Official Analytical Chemists (AOAC) , using a Chittick apparatus.[32] The gas-phase samples were determined by an infrared CO_2 gas analyzer (COZIR™ Wide Range) which enable to connect to computer and automatically collect data once per second.

5 Result and discussion

5.1 Model validation

A series of experiments were conducted to validate the proposed 2D- and 3D- models for membrane CO_2 absorption. A parity plot of the experimental and simulated values in terms of η was presented, as shown in **Figure 7**. It can be found that the 3D-based average absolute deviation (AAD) for the MC-1, MC-7 and MC-19 were 3.79%, 4.82% and 4.15%, respectively, which were favorably acceptable for MA simulation. By contrast, the 2D-based AAD for them were 9.82%, 21.31%, 28.05 %, respectively. Obviously, the 3D model provided better predicted results than the 2D model. It is also worth noting that the predicted values of the 2D model were overall higher than the experimental results as well as those of the 3D model. The reasons for the 2D prediction

deviations will be discussed in the next section.

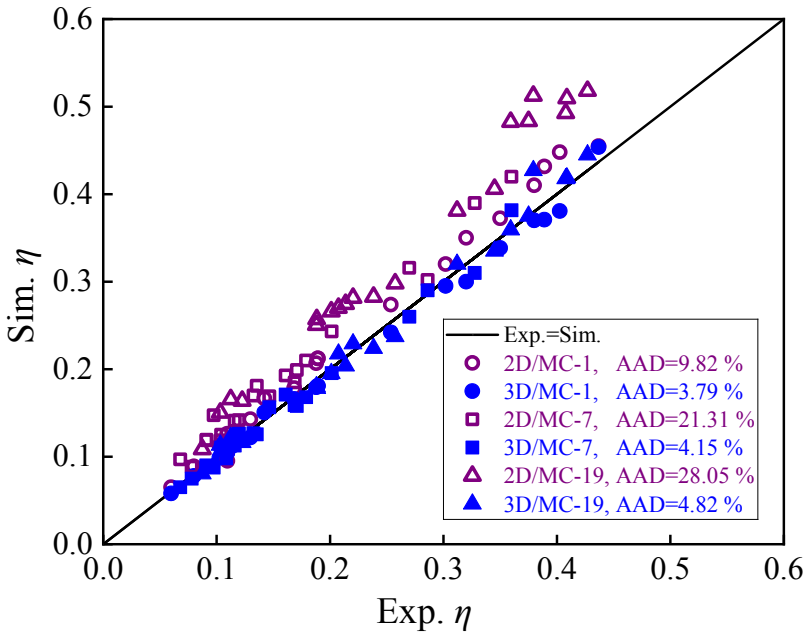

Figure 7. Comparison of 2D and 3D simulation results with experimental data for membrane absorption studies

To investigate the gas and liquid flow characterics in MCs, it is indispensable to validate the CFD simulations. **Figure 8a** shows the comparisons of the shell-side σ_θ^2 for the three MCs. It can be found that the simulated σ_θ^2 agree well with the experimental values. The AADs of them were 3.12%, 2.79% and 3.54%, respectively. **Figure 8b** shows the comparison between the RSD of liquid velocity of the simulated result and that of the expermental data for the MC-7 and the MC-19. The simulation results show good agreement with the experimental data, with AADs of 3.63% and 3.89%, respectively.

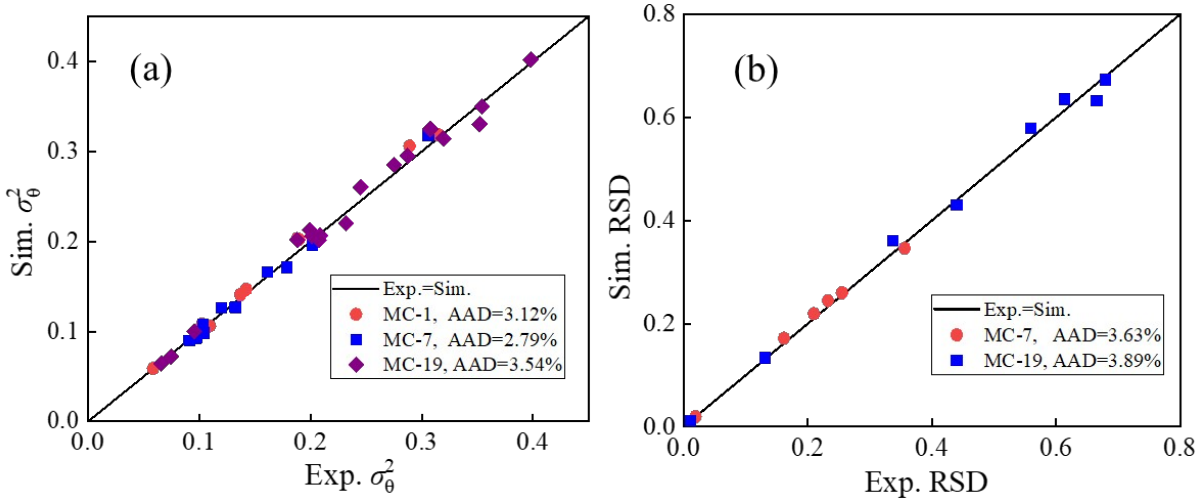

Figure 8. Comparison of simulation results and experimental data for (a) σ_θ^2 and (b) RSD

These comparisons indicated that the proposed 3D-based MA and CFD modelings performed in the COMSOL software were adequate and enabled reliable simulations. After the validation of the proposed 3D modeling approaches, more simulations can be carried out for wider ranges of operational conditions and membrane parameters. Furthermore, the 3D models can be employed for the formation of the geometry-related correction factor *F*.

5.2 Comparison between the 2D and 3D simulated flow characteristics

In this section, we attempted to clarify the prediction deviations between the 2D and 3D MA simulations from the perspective of geometry effect on flow characteristics. Simulations were performed using four MCs which had the same module length, membrane element sizes, packing density, gas and liquid velocities but different number of tubes. Based on the 2D modeling approach, as described in Section 3.1, the simulated flow characteristics of the four MCs were the same, and therefore can be represented with a case for illustration.

Let's conduct analysis from shell side flow characterics. It can be observed in **Figure 9** that the 2D velocity field showed typical features of laminar flow and the streamlines were straight and

parallel to the axial direction. These phenomena seem overly ideal and unreliable for all MCs. In fact, the nonideal phenomena of stagnant zone and bypassing become more and more serious as the number of membrane tubes increasing from 1 to 37, or in another words, with the decrease of the *H*/*D* ratio of the MCs. Stagnant zones exist, resulting in not only reduced effective membrane area for CO_2 mass transfer, but also longer renewal time for CO_2 modecules to diffuse in and out of these regions. Additionally, gas bypass increased the mixed degree of fluid particles in these MCs. Irregular velocity field was the main cause of nonuniform concentration field. **Figure 10** shows the gas-phase CO_2 concentration fields under different situations. Obviously, for the 2D case, the CO_2 concentration was monotone decreasing from inlet to the outlet. For the 3D cases, the CO_2 concentration became more and more complex. In the areas away from the inlet and outlet, the CO_2 concentration was lower than those nearby. Nonuniform CO_2 concentration distribution will increase the backmixing degree, which was undesirable for the MEA-CO_2 system (a second-order reaction).

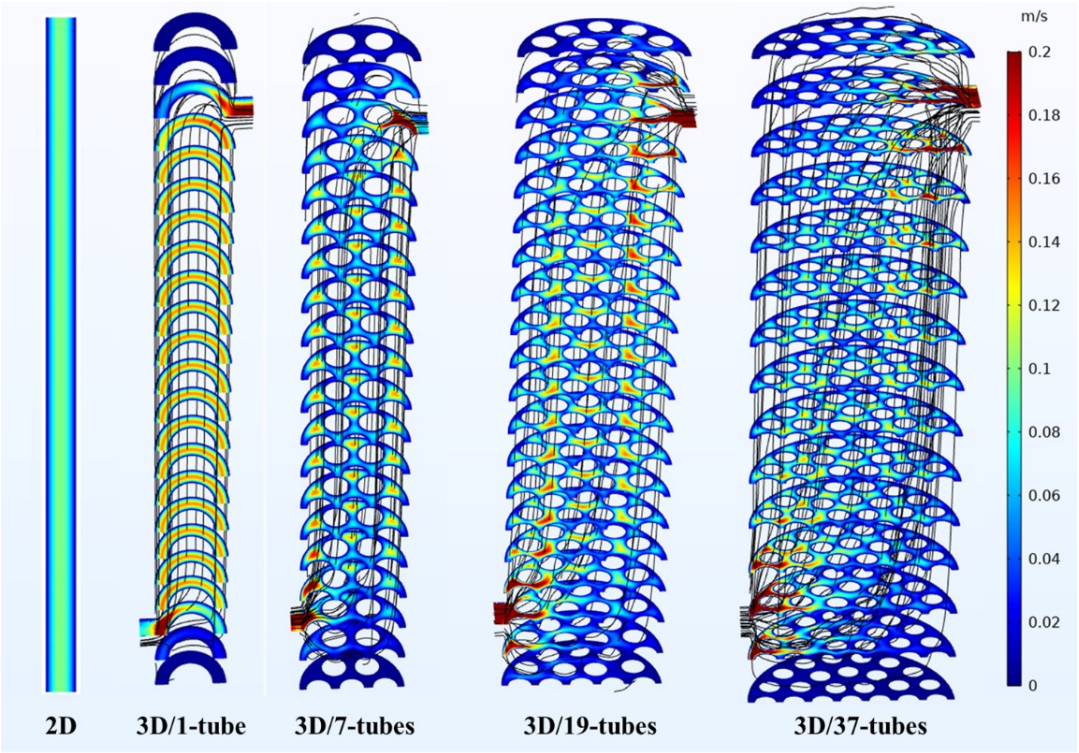

Figure 9. The 2D and 3D simulated velocity and streamline distributions in the shell side of various MCs.

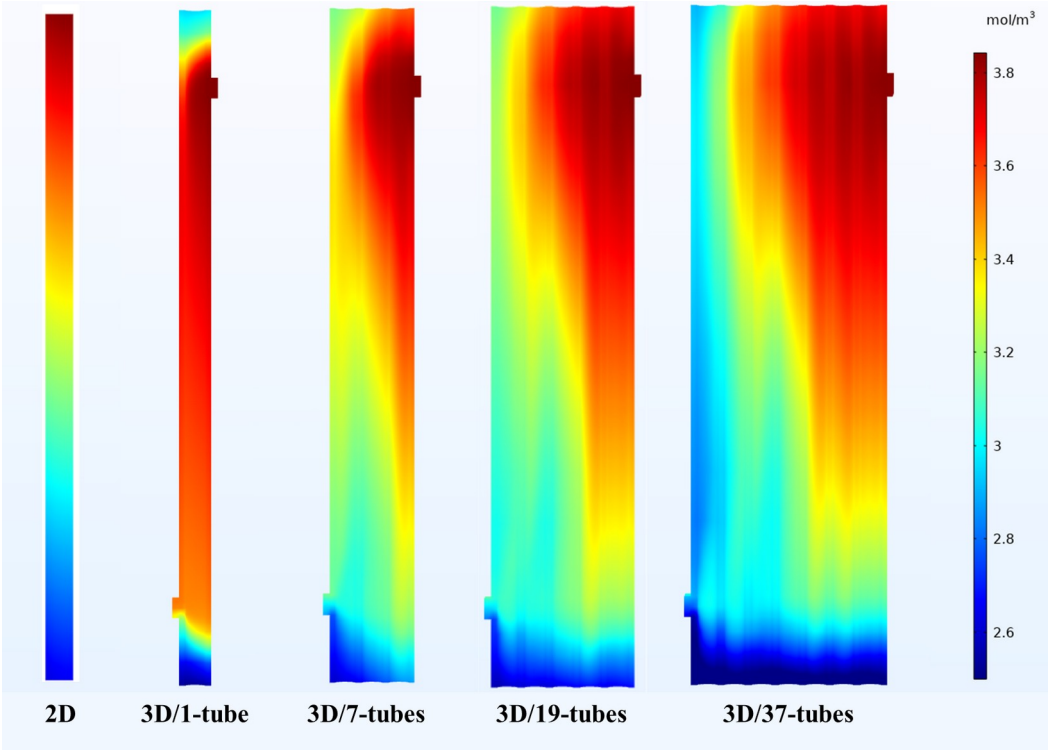

Figure 10. The 2D and 3D simulated CO_2 concentration distributions in the shell side of various MCs.

Figure 11 shows the 2D and 3D tube side flow characterics. The 2D flow characterics in the tube side were similar to that in the shell side. By comparison, the 3D simulation results were quite different. The liquid velocity was uniform inside an individual membrane tube since each tube has a large L/D ratio. More importantly, however, the principal problem was that of actual feed distribution to the individual tube, which was affected by the geometry of tube side entrance region. When the entrance size and the height of entrance region were the same for the four MCs, an increase in the membrane tubes led to worse feed distribution. As a result, the tubes close to the central region had high velocities than those in outer edges.

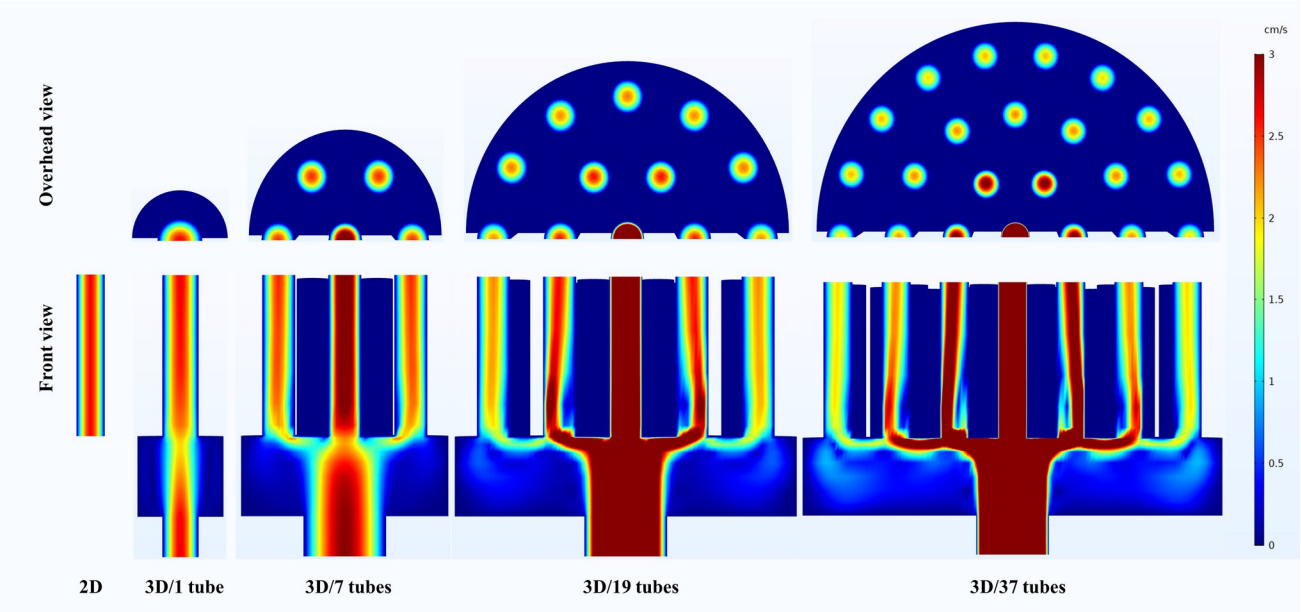

Figure 11. The 2D and 3D simulated liquid velocity distributions in the tube side entrance region of various MCs.

The above are the visual descriptions of the geometry effect on flow characterics under certain situations. Their characteristic parameters are listed in **Table 5**. Clearly, the σ_θ^2 of gas phase and the RSD of liquid phase in 2D case were approximately equal to zero; while those in 3D cases increased very rapidly as the number of membrane tubes increased. These results accounted for the prediction deviations of the 2D and 3D simulation results. Thus, design of new membrane contactors without consideration of geometry can lead to performance much worse than expectance based on 2D results.

Table 5 Comparison of 2D and 3D simulated fluid flow characteristics

Simulation cases	Shell side	Tube side
	σ_θ^2	RSD
2D	0.012	0
3D/1 tube	0.091	0
3D/7 tubes	0.145	0.162
3D/19 tubes	0.185	0.559
3D/37 tubes	0.216	0.983

5.3 Correlation for *F* prediction

To determine the F and to establish its prediction correlation, a series of simulations were performed varied in operating and MC parameters, including flow rates, temperature, concentrations, membrane length, tube number, the size and location of the inlet and outlet nozzles, et al., as presented in **Table 6**. The situations are complicated and diverse for such a multivariable system. Considering that this article focuses on the formation of the F, so here we will analyze the F at different σ_θ^2 and RSD situations rather than being exhaustive at various conditions of operation and MC geometry. For more information about how these factors affected σ_θ^2 and RSD, we will in-depth discuss in the next part of this series of articles.

Table 6. Geometrical characteristics and operating conditions used for simulations

Geometrical characteristics	Value	Operational conditions	Value
Tube number	1~37	Temperature (ºC)	25~50
Effective membrane length (m)	0.2~0.5	Pressure (kPa)	100
Tube inner diameter (mm)	1.0~8.0	Gas flow rate (L/min)	0.02~5.4
Membrane module diameter (mm)	3.0~100	CO_2 concentration (vol.%)	1~50
Overall membrane thickness (mm)	0.5~2.0	Liquid flow rate (ml/min)	5~1850
		MEA concentration (mol/L)	0.1~5.0
		CO_2 loading (mol/mol)	0~0.25

Here we proposed a correlation for the F which can be expressed in terms of a rational function (see Eq. 9), as a function of the σ_θ^2 and RSD, as well as operating parameters. Accordingly, the F was considered to be less than or equal to 1.

$$F = \frac{1}{1 + a\left(y_{A0}\right)^b \left(\sigma_\theta^2\right)^c + d\left(\frac{\nu_B F_{A0}}{\nu_A F_{B0}}\right)^e \left(\mathrm{RSD}\right)^f} \tag{9}$$

where y_{A0} is the initial CO_2 concentration in gas phase; F_{A0} and F_{B0} are the initial mole flow rates of CO_2 and effective MEA, mol/min; ν_A and ν_B are the stoichiometric coefficients of A and B, respectively.

To check against applicability of the predictive correlation of F, the plot of the desired F obtained from the η_{3D}/η_{2D} vs that calculated from Eq. 9 was investigated, as shown in **Figure 12**. Through data fitting, a set of optimum values of a~f in Eq. 9 were found to be 4.46, 0.52, 1.09, 0.23, 0.72 and 0.86, respectively. Thus, the F can be written as Eq. 10. The corresponding AAD was found to be 4.92 %, which is favorably acceptable for MA prediction.

$$F = \frac{1}{1+4.46\left(y_A\right)^{0.52}\left(\sigma_\theta^2\right)^{1.09}+0.23\left(\frac{\nu_B F_{A0}}{\nu_A F_{B0}}\right)^{0.72}\left(\mathrm{RSD}\right)^{0.86}} \tag{10}$$

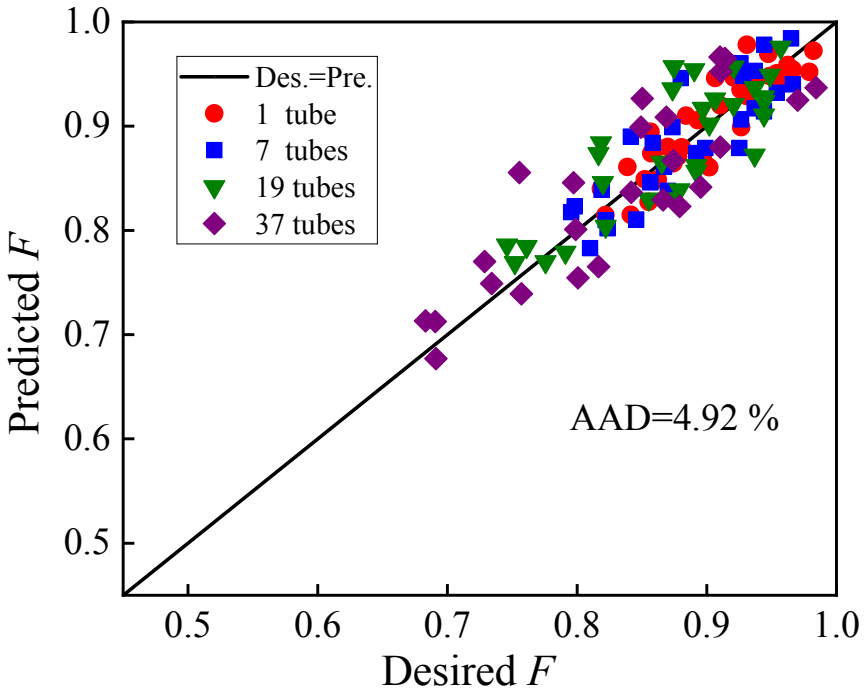

Figure 12. Crossplot between desired and predicted *F* values.

To validate the accuracy of Eq. 10, the simulated results presented in tems of $\eta_{hybrid}=\eta_{2D}\cdot F$ were compared with the the η_{exp}. The parity plot in **Figure 13** shows that the η_{hybrid} were in good agreement with the η_{exp} values, with AAD of 4.38%, which demonstrates that this hybrid modeling approach can be successfully applied.

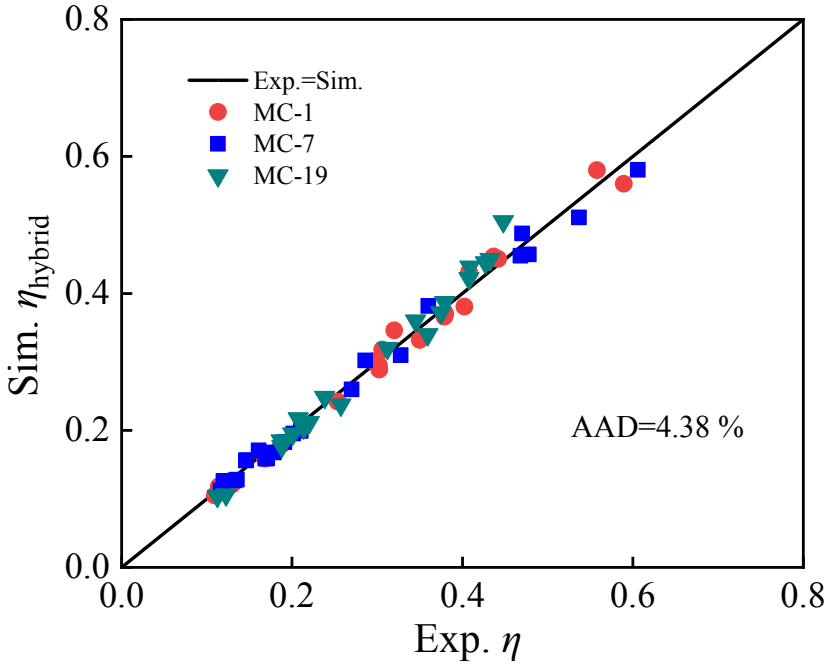

Figure 13. Crossplot between the simulated results obtained from the hybrid modeling and the experimental data.

5.4 Advantages of the hybrid model over the 3D MA model

It has been demonstrated that both the 3D and the hybrid models are reliable for the MA-CO_2 simulation. The 3D model tended to be more accurate because its modeling process was more in line with the actual situations. However, it still suffers from the computation accuracy versus efficiency trade-off. Here we aim to place several common and important considerations in numerial simulation and MA studies and try to explain the advantages of the hybrid models over the 3D MA model.

Consideration I: Convergence problems. Typical MA processes under co-current operation are nonlinear boundary value problems (BVPs) which are much more difficult to solve and more demanding than initial value problems (IVPs) from the point of numerical simulation. The approach to solving BVPs requires iterative "guess" and "feedback" of exit information and will take considerable computation time to converge. Unfortunately, the problems of slow convergence or

non-convergence are often encountered when a complex system is involved, just as the reactive membrane absorption of CO_2 in large complex MCs. Modeling and simulation of such complex system in 3D case requires considerable meshes for discretization, dramatically increases the demand for computational resources. Worse, irregular geometry complicates flow behaviors in MCs, leading to difficult convergence. The hybrid model, combining a 2D MA model with a 3D CFD model, is an advanced approach by disaggregating the influence of reactive MA process and complex geometry. A 2D axial symmetry geometry requires much less meshes for discretization and allows fluids to flow more regular compared to the 3D geometry. So the 2D MA model, which involves a complex process and a simple geometry, is expected to be more easy to converge and particularly suitable to evaluate the performance of absorbent and membrane. Although the 3D CFD model involves complex geometry, it is an IVP and involves only convective mass transfer. Similarly, the 3D CFD model is simpler than the 3D MA model and particularly suitable to investigate the geometry effect and to design and optimize tube arrangement and module configuration.

Consideration II: Computational efficiency for sensitivity analysis of key parameters. To design and optimize MCs for CO_2 capture, the effects of different key operating and membrane parameters on the MA performance should be comprehensively investigated, including the flow rates, temperatures and components of gas and liquid phases, as well as membrane pore size, and so on. Any change of key parameters may result in different MA performance. Therefore, extensive simulations should be performed to find suitable design and actual operating conditions and membrane properties. As a result, how to address batch simulation accurately and efficiently is essential. For example, estimating the MA-CO_2 performance at conditions of 5 different gas flow rates and 5 different liquid flow rates, these exist 25 combinations. If the 3D MA simulation is

performed for every combination, it will be an incredibly inefficient use of computing resources. Using the hybrid model to achieve the simulation task, it needs 25 runs of 2D MA simulation, as well as 25 different *F* values which can be obtained by combining 5 sets of gas CFD data and 5 sets of liquid CFD data with each other. Considering that the 2D MA and 3D CFD simulations are much easier and require less time compared to the 3D MA simulation, the hybrid model is more flexible and efficient. Hence, it is very helpful in batch simulation work in which the sensitivities of a number of significant variables need to be analyzed.

Consideration III: An ability to perform time-dependent MA simulation. Membrane wetting is considered as a challenging problem in MC. It arises from liquid absorbents entrying into membrane pores gradually, and will lead to the increase in membrane resistance, and thus a reduction in MA performance. To investigate the influence of various parameters on membrane wetting, it may be necessary to perform transient MA simulations and then validated their results with experimental data. Since the required computation load and time for a transient simulation are much higher than those for a steady simulation, such transient simulations can hardly performed in 3D case. In this case, the 2D MA model can be a good choice for the membrane wetting investigation. The *F* is not affected by the membrane wetting process and can be applied to correct the geometry geometry.

Overall, the hybrid model offers efficient and flexible ways to simulate the MA process without sacrificing the required accuracy. This contributes to higher accuracy-efficiency conbinations, but still needs more experimental data, expecially pilot or large-scale data, to enhance its accuracy and applicability.

Conclusion

In this work, geometry effect on membrane absorption for CO_2 capture has been demonstrated

by experimental and simulation studies. It was also found that the proposed 3D model, with AADs of 3.79%, 4.15% and 4.82% for the MC-1, MC-7 and MC-19, respectively, provided better predicted results than the conventional 2D model, with AADs of 9.82 %, 21.31% and 28.05% for the three MCs, respectively. More importantly, a new hybrid modeling approach was successfully developed to improve the simulation efficiency and verified by comparison of its results with the experimental data, with AAD of 4.38%. It is particularly suitable for the simulation of reactive membrane absorption in membrane contctors with complex geometry.

However, while this hybrid modeling approach has great advantages, a significant challenge must also be addressed, i.e., how to obtain effectively required flow characteristic parameters. It is still a very hard work to perform 3D modeling and simulation. To save time and improve the utilization of computing resources, therefore, in the next part of this series of articles, we attempt to develop correlations for predicting the σ_θ^2 and RSD parameters under various operating and geometrical variables.

Notation

C	concentration	mol/m^3
Cp	specific heat	J/(mol·K)
D	diffusion coefficient	m^2/s
F	correction factor	
ΔH_{abs}	heat of absorption	
He	henry's constant	kPa·m^3/kmol
k_i	reaction rate constant	
P	pressure	Pa
Q	flow rate	mL/min
R	ideal gas constant	J/(mol·K)
RSD	relative standard deviation	
T	temperature	K
U	velocity	m/s

ρ	density	kg/m^3
η	removal efficiency	%
μ	viscosity	Pa·s
λ	thermal conductivity	W/(m·K)
γ	surface tension	N/m

Acknowledge

This study was financially supported by the National key R&D plan (2016YFC0205700), the National Natural Science Foundation of China (21706114), National Students' platform for innovation and entrepreneurship training program (202010291065Z), the Project of Priority Academic Program Development of Jiangsu Higher Education Institutions (PAPD).

References

1. Zhao S, Feron PH, Deng L, et al. Status and progress of membrane contactors in post-combustion carbon capture: A state-of-the-art review of new developments. *J. Membr. Sci.* 2016;511:180-206.

2. Chabanon E, Favre E. 3.9 Membranes Contactors for Intensified Gas–Liquid Absorption Processes. In: Drioli E, Giorno L, Fontananova E, eds. *Comprehensive Membrane Science and Engineering (Second Edition)*. Oxford: Elsevier; 2017:249-281.

3. Xu P, Huang Y, Kong X, et al. Hydrophilic membrane contactor for improving selective removal of SO_2 by NaOH solution. *Sep. Purif. Technol.* 2020/11/01/ 2020;250:117134.

4. Hosseinzadeh A, Hosseinzadeh M, Vatani A, Mohammadi T. Mathematical modeling for the simultaneous absorption of CO_2 and SO_2 using MEA in hollow fiber membrane contactors. *Chemical Engineering and Processing-Process Intensification.* Jan 2017;111:35-45.

5. Cao F, Gao H, Li H, Liang Z. Experimental and theoretical studies on mass transfer performance for CO_2 absorption into aqueous N,N-dimethylethanolamine solution in the polytetrafluoroethylene hollow-fiber membrane contactor. *Ind. Eng. Chem. Res.* 2018;57(49):16862-16874.

6. Cao F, Gao H, Gao G, Liang Z. Mass transfer performance and correlation for CO_2 absorption into aqueous 1-dimethylamino-2-propanol (1DMA2P) solution in a PTFE hollow fiber membrane contactor. *Chem. Eng. Process.* 2019;136:226-233.

7. Wang F, Kang G, Liu D, Li M, Cao Y. Enhancing CO_2 absorption efficiency using a novel PTFE hollow fiber membrane contactor at elevated pressure. *AlChE J.* Jun 2018;64(6):2135-2145.

8. Gao G, Gao HX, Liang ZW. Mass transfer performance and correlations for CO_2 absorption into aqueous blended PG/MEA in PTFE membrane contactor. *J. Chem. Technol. Biotechnol.* Jan 2020;95(1):27-39.

9. Cao F, Gao H, Ling H, Huang Y, Liang Z. Theoretical modeling of the mass transfer performance of CO_2 absorption into DEAB solution in hollow fiber membrane contactor. *J. Membr. Sci.* 2020;593:117439.

10. Liang W, Chenyang Y, Bin Z, et al. Hydrophobic polyacrylonitrile membrane preparation and its use in membrane contactor for CO_2 absorption. *J. Membr. Sci.* 2019/01/01/ 2019;569:157-165.

11. Qiu MH, Kong XL, Fu KY, et al. Optimization of microstructure and geometry of hydrophobic ceramic membrane for SO_2 absorption from ship exhaust. *AlChE J.* 2019;65(1):409-420.

12. Fougerit V, Pozzobon V, Pareau D, Theoleyre MA, Stambouli M. Experimental and numerical investigation binary mixture mass transfer in a gas -liquid membrane contactor. *J. Membr. Sci.* 2019;572:1-11.

13. Li S, Pyrzynski TJ, Klinghoffer NB, et al. Scale-up of PEEK hollow fiber membrane contactor for post-combustion CO_2 capture. *J. Membr. Sci.* 2017;527(527):92-101.

14. Hoff KA, Svendsen HF. Membrane contactors for CO_2 absorption – Application, modeling and mass transfer effects. *Chem. Eng. Sci.* 2014/09/06/ 2014;116:331-341.

15. Zaidiza DA, Wilson SG, Belaissaoui B, et al. Rigorous modelling of adiabatic multicomponent CO_2 post-combustion capture using hollow fibre membrane contactors. *Chem. Eng. Sci.* May 12 2016;145:45-58.

16. Zaidiza DA, Billaud J, Belaissaoui B, Rode S, Roizard D, Favre E. Modeling of CO_2 post-combustion capture using membrane contactors, comparison between one- and two-dimensional approaches. *J. Membr. Sci.* 2014;455:64-74.

17. Caplow M. Kinetics of carbamate formation and breakdown. *J. Am. Chem. Soc.* 1968;90(24):6795-6803.

18. Danckwerts P. The reaction of CO_2 with ethanolamines. *Chem. Eng. Sci.* 1979;34(4):443-446.

19. Hagewiesche DP, Ashour SS, Al-Ghawas HA, Sandall OC. Absorption of carbon dioxide into aqueous blends of monoethanolamine and *N*-methyldiethanolamine. *Chem. Eng. Sci.* 1995;50(7):1071-1079.

20. Welty JR, Wicks CE, Rorrer G, Wilson RE. *Fundamentals of momentum, heat, and mass transfer*: John Wiley & Sons; 2009.

21. Weiland RH, Dingman JC, Cronin DB. Heat capacity of aqueous monoethanolamine, diethanolamine, N-

methyldiethanolamine, and N-methyldiethanolamine-based blends with carbon dioxide. *J. Chem. Eng. Data.* Sep-Oct 1997;42(5):1004-1006.

22. Versteeg G, Van Swaaij WPM. Solubility and diffusivity of acid gases (carbon dioxide, nitrous oxide) in aqueous alkanolamine solutions. *Journal of Chemical & Engineering Data.* 1988;33(1):29-34.

23. Ko JJ, Tsai TC, Lin CY, Wang HM, Li MH. Diffusivity of nitrous oxide in aqueous alkanolamine solutions. *J. Chem. Eng. Data.* Jan-Feb 2001;46(1):160-165.

24. Kim I, Svendsen HF. Heat of absorption of carbon dioxide (CO_2) in monoethanolamine (MEA) and 2-(aminoethyl) ethanolamine (AEEA) solutions. *Ind. Eng. Chem. Res.* 2007;46(17):5803-5809.

25. Perry RH, Green D, Maloney J. Perry's Handbook of Chemical Engineering 7th ed. *McGraw-Hill Book Company: New York.* 1997.

26. Weiland RH, Dingman JC, Cronin DB, Browning GJ. Density and viscosity of some partially carbonated aqueous alkanolamine solutions and their blends. *J. Chem. Eng. Data.* 1998;43(3):378-382.

27. Vázquez G, Alvarez E, Navaza JM, Rendo R, Romero E. Surface tension of binary mixtures of water+ monoethanolamine and water+ 2-amino-2-methyl-1-propanol and tertiary mixtures of these amines with water from 25 °C to 50 °C. *J. Chem. Eng. Data.* 1997;42(1):57-59.

28. Hikita H, Asai S, Ishikawa H, Honda M. The kinetics of reactions of carbon dioxide with monoethanolamine, diethanolamine and triethanolamine by a rapid mixing method. *Chem. Eng. J.* 1977;13(1):7-12.

29. Edwards TJ, Maurer G, Newman J, Prausnitz JM. Vapor-liquid-equilibria in multicomponent aqueous-solutions of volatile weak electrolytes. *AlChE J.* 1978;24(6):966-976.

30. Glasscock DA, Critchfield JE, Rochelle GT. CO_2 absorption/desorption in mixtures of methyldiethanolamine with monoethanolamine or diethanolamine. *Chem. Eng. Sci.* 1991;46(11):2829-2845.

31. Gao N, Li M, Jing W, Fan Y, Xu N. Improving the filtration performance of ZrO_2 membrane in non-polar organic solvents by surface hydrophobic modification. *J. Membr. Sci.* 2011;375(1-2):276-283.

32. Horwitz W. Association of official analytical chemists (AOAC) methods 12th ed. *George Banta Company, Menasha, WI.* 1975.